

Strong dependence of band-gap opening at the Dirac point of graphene upon hydrogen adsorption periodicity

J. M. García-Lastra

Nano-Bio Spectroscopy Group and ETSF Scientific Development Centre, Depto. Física de Materiales, Universidad del País Vasco, Avenida de Tolosa 72, E-20018 San Sebastián, Spain

and Center for Atomic-scale Materials Design, Department of Physics, Technical University of Denmark, DK-2800 Kongens Lyngby, Denmark

(Received 28 September 2010; published 10 December 2010)

The band gap of periodically doped graphene with hydrogen is investigated. It is found through a tight-binding (TB) model that for certain periodicities, called here nongap periodicities (NGPs), no gap is opened at the Dirac point. Density-functional-theory calculations show that a tiny gap is opened for NGPs due to exchange effects, not taken into account in the TB model. However, this tiny gap is one order of magnitude smaller than the gap opened for other periodicities different from NGPs. This remarkable reduction in the band-gap opening for NGPs provokes a crossing of the midgap and the conduction bands and, consequently, the metallization of the system. This result is also valid for other adsorbates different from atomic hydrogen.

DOI: 10.1103/PhysRevB.82.235418

PACS number(s): 61.46.–w, 71.15.Nc, 73.22.Dj

The unusual semimetallic behavior of graphene, a single layer of graphite, was first studied theoretically by Wallace¹ and its recent synthesis² has renewed the interest for this material.³ The great variety of physical and chemical properties derived from the electronic structure of graphene makes it very attractive for a range of applications, from catalysis⁴ to nanoscale electronics.⁵ It is remarkable that graphene is a gapless semiconductor, with no gap at the Dirac point³ [the K and K' points in Fig. 1(b)]. However, it is well known that the presence of defects such as vacancies or impurities,^{6,7} the interaction with a substrate,⁸ or the edge structure (in graphene nanoribbons)^{9–11} can lead to a band-gap opening in graphene.³

In particular, the hydrogenation of graphene and its effect in the band gap has been investigated in several recent works.^{9,11–20} Combined scanning tunneling microscopy and angle-resolved photoemission spectroscopy experiments showed that the patterned adsorption of atomic hydrogen onto the Moiré superlattice positions of graphene grown on an Ir(111) substrate produces a band-gap opening in graphene.¹² Density-functional-theory (DFT) calculations reported in the literature^{14,17,21} also predict a band-gap opening, which depends on the periodicity of the hydrogen adsorption, namely: (i) in graphene, the fully hydrogenated graphene, the gap at the Γ point [see Fig. 1(b)] is 3.5 eV, whereas the gap opening at the Dirac point is above 10 eV.²¹ (ii) In half-hydrogenated graphene the maximum of the valence band is at the Dirac point and the minimum of the conduction band is at the Γ point with a gap between them of 0.43 eV. The direct gap at the Dirac point is 1.16 eV.¹⁷ (iii) In a graphene sheet with a hydrogen atom adsorbed with a $4\vec{a}_1 \times 4\vec{a}_2$ periodicity, being \vec{a}_1 and \vec{a}_2 the basis vectors of the hexagonal lattice of graphene [see Fig. 1(a)], the gap opened at the Dirac point, which in this case is the gap of the material, is 1.25 eV.¹⁴ In this case a midgap state (a localized state in the vicinity of the H atom) appears 0.45 eV above the valence band.¹⁴

After these observations the following question arises: does the periodical adsorption of hydrogen atoms in

graphene lead to an opening of its gap for any periodicity? In order to answer this question we will first examine the main features of the structure of graphene and its reciprocal lattice, depicted in Fig. 1. A graphene sheet consists of a two-dimensional hexagonal lattice with two atoms per unit cell [A and B atoms in Fig. 1(a)]. The p_z orbitals of the carbon atoms, which cannot overlap with p_x , p_y , or s orbitals (it is forbidden by symmetry), form π bands. We can understand the band structure of graphene through a tight-binding (TB) model, making linear combinations of the p_z orbitals of A and B atoms, denoted here as p_z^A and p_z^B , respectively. The corresponding TB Hamiltonian for the unit cell of graphene, assuming the overlap between p_z^A and p_z^B orbitals to be negligible, can be written as

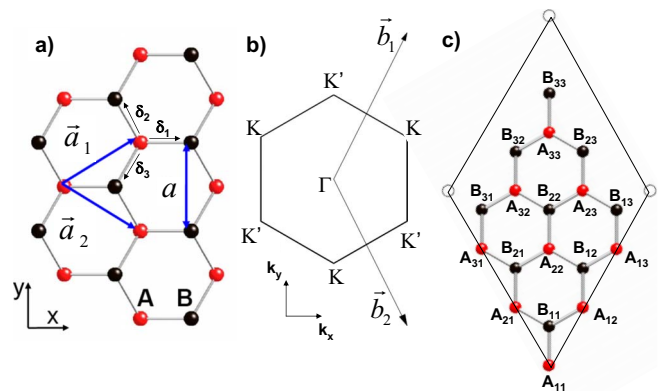


FIG. 1. (Color online) (a) Basis vectors of the hexagonal lattice of graphene, $\vec{a}_{1,2} = \frac{a}{2}(\sqrt{3}, \pm 1)$, with $a = \sqrt{3}d_{C-C}$, being d_{C-C} the carbon-carbon distance. Atoms in A(B) sites are in red (black). The coordinates of the A and B sites in the unit cell at the origin are $(0,0)$ and $1/3(\vec{a}_1 + \vec{a}_2)$, respectively. $\vec{\delta}_1 = (\frac{a}{\sqrt{3}}, 0)$, $\vec{\delta}_2 = (-\frac{a}{2\sqrt{3}}, \frac{a}{2})$, and $\vec{\delta}_3 = (-\frac{a}{2\sqrt{3}}, -\frac{a}{2})$ are the nearest-neighbor vectors. (b) The first Brillouin zone of graphene with the K and K' points at $K', K = (0, \pm 4\pi/3a)$. (c) A $3 \cdot \vec{a}_1 \times 3 \cdot \vec{a}_2$ supercell showing the criterion for the labeling of the carbon atoms followed in the present work.

$$\begin{pmatrix} \varepsilon_0 & -\gamma_0 f(\vec{k}) \\ -\gamma_0 f^*(\vec{k}) & \varepsilon_0 \end{pmatrix} \begin{pmatrix} c_A(\vec{k}) \\ c_B(\vec{k}) \end{pmatrix} = E(\vec{k}) \begin{pmatrix} c_A(\vec{k}) \\ c_B(\vec{k}) \end{pmatrix}, \quad (1)$$

where γ_0 is the transfer integral between first-neighbor p_z orbitals [a typical value for it is 2.9 eV (Ref. 22)], ε_0 is the energy reference from the p_z orbital of a carbon atom (which in the following will be set to $\varepsilon_0=0$), and the phase factor is $f(\vec{k}) = \sum_{\vec{\delta}_j=1}^3 e^{i\vec{k}\cdot\vec{\delta}_j}$, being $\vec{\delta}_j$ the nearest-neighbors vectors (see Fig. 1). $c_A(\vec{k})$ and $c_B(\vec{k})$ are, respectively, the coefficients of p_z^A and p_z^B orbitals in the linear combinations of the eigenfunctions. It can be noticed that at $\vec{k}=\vec{K}, \vec{K}'$, i.e., at the Dirac

points, $f(\vec{k})=0$. Thus at the Dirac point, p_z^A and p_z^B orbitals are decoupled and degenerate in energy, leading to a zero-gap semiconductor band structure.

The same TB scheme can be used to model a $m\cdot\vec{a}_1 \times n\cdot\vec{a}_2$ graphene supercell (SC), instead of the $\vec{a}_1 \times \vec{a}_2$ unit cell used in Eq. (1). The TB Hamiltonian of a $m\cdot\vec{a}_1 \times n\cdot\vec{a}_2$ SC at the Dirac point is a Hermitian matrix full of zeros, except for the coupling matrix elements between two nearest neighbors. These coupling matrix elements for two atoms connected by $\vec{\delta}_1$, $\vec{\delta}_2$, and $\vec{\delta}_3$ are $-\gamma_0$, $-\gamma_0 \cdot e^{2\pi i/3}$, and $-\gamma_0 \cdot e^{-2\pi i/3}$ (and their respective conjugated), respectively. For instance, the corresponding TB Hamiltonian for a $2\cdot\vec{a}_1 \times 2\cdot\vec{a}_2$ SC at the Dirac point is

$$-\gamma_0 \begin{pmatrix} 0 & 1 & 0 & e^{i2\pi/3} & 0 & e^{-i2\pi/3} & 0 & 0 \\ 1 & 0 & e^{-i2\pi/3} & 0 & e^{i2\pi/3} & 0 & 0 & 0 \\ 0 & e^{i2\pi/3} & 0 & 1 & 0 & 0 & 0 & 0 \\ e^{-i2\pi/3} & 0 & 1 & 0 & 0 & 0 & e^{i2\pi/3} & 0 \\ 0 & e^{-i2\pi/3} & 0 & 0 & 0 & 1 & 0 & e^{i2\pi/3} \\ e^{i2\pi/3} & 0 & 0 & 0 & 1 & 0 & e^{-i2\pi/3} & 0 \\ 0 & 0 & 0 & e^{-i2\pi/3} & 0 & e^{i2\pi/3} & 0 & 1 \\ 0 & 0 & e^{i2\pi/3} & 0 & e^{-i2\pi/3} & 0 & 1 & 0 \end{pmatrix} \begin{pmatrix} A_{11} \\ B_{11} \\ A_{12} \\ B_{12} \\ A_{21} \\ B_{21} \\ A_{22} \\ B_{22} \end{pmatrix} = E \begin{pmatrix} A_{11} \\ B_{11} \\ A_{12} \\ B_{12} \\ A_{21} \\ B_{21} \\ A_{22} \\ B_{22} \end{pmatrix}, \quad (2)$$

where A_{ij} and B_{ij} are, respectively, the coefficients of p_z^A and p_z^B orbitals at the position $i\cdot\vec{a}_1 \times j\cdot\vec{a}_2$ in the linear combinations of the eigenfunctions [see Fig. 1(c) for the labeling of the carbon atom sites].

Obviously, the band gap at the Dirac point has to be (and it is) independent of the choice of the $m\cdot\vec{a}_1 \times n\cdot\vec{a}_2$ graphene SC. For any size of the SC the highest occupied level (HOL) and the lowest unoccupied level (LUL) are degenerate with zero energy. HOL corresponds to the linear combination with all $A_{ij}=0$ and all $B_{ij}=1$. LUL corresponds to the linear combination with all the coefficients $A_{ij}=1$ and all the coefficients $B_{ij}=0$ (since the levels are degenerate, this correspondence is arbitrary and could be the opposite). However, if the size of the SC is $m\cdot\vec{a}_1 \times n\cdot\vec{a}_2$, being *both* m and n multiple of 3 (in the following this sort of SCs will be referred as 3C-SCs) a new feature arises: the second highest occupied level (HOL-1) and the second lowest unoccupied one (LUL+1) are also degenerate with the HOL and the LUL. This is because both inequivalent Dirac points, \vec{K} and \vec{K}' , of the graphene Brillouin zone are coincident with the Γ point of a 3C-SC reciprocal cell. Thus, the solutions of the TB Hamiltonian for a 3C-SC at the \vec{K} point also include the solutions at the \vec{K}' point. For this reason there are four degenerate states with energy 0 for a 3C-SC, instead of the two found for the non-3C-SCs. In the case of non-3C-SCs the positions of \vec{K} and \vec{K}' points remain inequivalent. This feature can be better understood by looking at Fig. 2, where the reciprocal lattices of a $3\cdot\vec{a}_1 \times 3\cdot\vec{a}_2$ SC (a 3C-SC) and a $4\cdot\vec{a}_1 \times 4\cdot\vec{a}_2$ SC (a non-3C-SC) are shown.

In the case of a 3C-SC the HOL and the LUL are the same as in the case of a non 3C-SC. However, since HOL and LUL are degenerate with the HOL-1 and the LUL+1 in a 3C-SC, it is possible to form new linear combinations of them that are also eigenfunctions of the Hamiltonian. For convenience, the following orthogonal linear combinations will be taken:

$$\begin{aligned} \text{HOL} - 1 &\rightarrow \text{All } B_{ij}=0; A_{ij}^3=1; A_{ij}^2=0; A_{ij}^1=e^{i\pi/3}, \\ \text{HOL} &\rightarrow \text{All } A_{ij}=0; B_{ij}^3=1; B_{ij}^2=0; B_{ij}^1=e^{i\pi/3}, \\ \text{LUL} &\rightarrow \text{All } A_{ij}=0; B_{ij}^3=0; B_{ij}^2=1; B_{ij}^1=e^{-i\pi/3}, \\ \text{LUL} + 1 &\rightarrow \text{All } B_{ij}=0; A_{ij}^3=0; A_{ij}^2=1; A_{ij}^1=e^{-i\pi/3}, \end{aligned} \quad (3)$$

where the superscripts 3, 2, and 1 in the A_{ij} and B_{ij} coefficients mean that $(i-j)$, $(i-j-2)$, and $(i-j-1)$ are multiple of 3, respectively.

The main effects of the adsorption of hydrogen atom in a site X of the graphene sheet are two, namely: (i) the potential of the H^+ ionic core shifts the energy of site X with respect to the rest of the carbon atoms.¹⁴ This effect can be introduced straightforwardly in the TB model, just by adding a potential energy, V , to the diagonal element of the site X in the TB matrix. (ii) After the adsorption, the carbon atom at site X is fourfold coordinated, so its hybridization changes from sp^2 to sp^3 . This leads to a change in the transfer integral with its

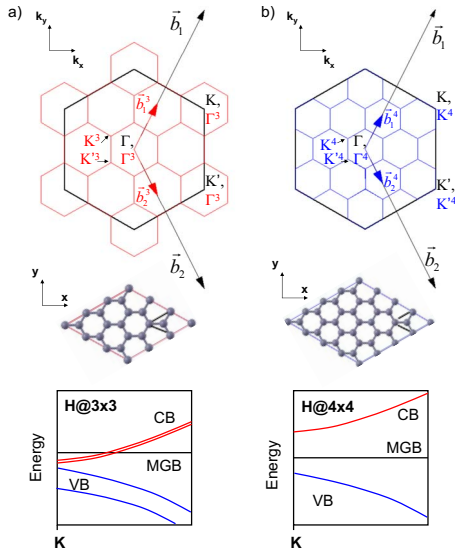


FIG. 2. (Color online) (a) Top: Brillouin zones of a 1×1 (black) and 3×3 (red) supercells of graphene. $\vec{b}_{1,2}$ and $\vec{b}_{3,2}$ are the reciprocal basis vectors of the 1×1 and 3×3 (red) supercells, respectively. High symmetry points of 1×1 Brillouin zone are in black without any superscript. The high symmetry points of 3×3 Brillouin zone are in red with a 3 superscript. Middle: the 3×3 supercell. Bottom: schematics of the band structure of a 3×3 supercell upon adsorption of a hydrogen atom in the vicinity of the Dirac point, showing the valence band (VB), conduction band (CB), and midgap band (MGB). (b) Brillouin zones of a 1×1 (black) and 4×4 (blue) supercells of graphene. $\vec{b}_{1,2}$ and $\vec{b}_{4,2}$ are the reciprocal basis vectors of the 1×1 and 4×4 (blue) supercells, respectively. High symmetry points of 1×1 Brillouin zone are in black without any superscript. The high symmetry points of 4×4 Brillouin zone are in blue with a 4 superscript. Middle: the 4×4 supercell. Bottom: schematics of the band structure of a 4×4 supercell upon adsorption of a hydrogen atom in the vicinity of the Dirac point.

first neighbors.^{3,7,11,18} In the TB model this is accounted for by replacing the factor γ_0 in the coupling matrix elements of site X by a factor γ_H . Here, without losing generality, it will be considered that the adsorption of the H atom occurs at the A_{11} site. In a non-3C-SC the HOL of the pristine graphene remains an eigenfunction of the doped system since the coefficient $A_{11}=0$. By contrast, the LUL of the pristine graphene is not anymore an eigenfunction of the doped system since the coefficient $A_{11}=1$. Consequently, the HOL and

the LUL are not anymore degenerate in a non-3C-SC and a gap is opened at the Dirac point. This result of the TB model is confirmed by the DFT calculations of Duplock *et al.*¹⁴ for a $4\vec{a}_1 \times 4\vec{a}_2$ SC, where they found an opening in the gap of 1.25 eV. The TB model also predicts the size of the gap between the HOL and the LUL in a non-3C-SC to be proportional to $\frac{1}{m \cdot n}$, i.e., the gap is proportional to the hydrogen concentration. This result can be checked using the MATLAB code given in Ref. 23. Martinazzo *et al.*¹⁸ found the same proportional law for graphene supercells doped with two H atoms, one in the sublattice A and the other in the sublattice B.

In a 3C-SC the HOL, LUL, and LUL+1 shown in Eq. (3) have a coefficient $A_{11}=0$ and hence they remain eigenfunctions of the TB Hamiltonian after the H atom adsorption. It can be verified that the change in the coupling matrix elements of the A_{11} site from γ_H to γ_0 does not affect to this result. The HOL-1 has a coefficient $A_{11}=1$ and thus is not anymore an eigenfunction after the adsorption. However, since three of the four frontier levels in a 3C-SC remain unaffected after the H adsorption it can be concluded that no gap is opened at the Dirac point after the adsorption of one H atom in a 3C-SC. Moreover, since all the coefficients A_{ij} are equal to zero for the HOL-1, HOL, and LUL, the following more general conclusion can be reached: *it is possible to adsorb several H atoms in a 3C-SC without a band gap opening at the Dirac point if all the H atoms are adsorbed at A_{ij} sites, being $(i-j)$ multiple of 3.* Henceforth this sort of arrangement will be called NGPs (nongap periodicities). Given that V and γ_H are adjustable parameters dependent on the kind of adsorbate, this result is also valid for other adsorbates different from atomic hydrogen.

It should be mentioned that Zhang *et al.*,²⁴ through the Born approximation for pointlike scattering potentials, and García-Lastra *et al.*,²⁵ by means of the nonequilibrium Green's function formalism, studied the ballistic transport of electrons in carbon nanotubes (CNTs). They found that for certain arrangements of two or more adsorbates on CNTs, which are particular cases of the NGPs presented here, there is an open channel close to the Fermi level for the electronic transport. That result is physically equivalent to the nonband-gap opening result shown in this work.

In order to validate the results of the TB model for the 3C-SCs, spin-polarized DFT calculations on $3\vec{a}_1 \times 3\vec{a}_2$, $6\vec{a}_1 \times 3\vec{a}_2$, $9\vec{a}_1 \times 3\vec{a}_2$, $12\vec{a}_1 \times 3\vec{a}_2$, and $6\vec{a}_1 \times 6\vec{a}_2$ SCs (all of them

TABLE I. DFT energies (in eV) with respect to the Fermi level of the four frontier bands at the Dirac point for a graphene sheet with one hydrogen atom adsorbed with 3×3 , 6×3 , 9×3 , 12×3 , and 6×6 periodicities. $S\uparrow$ and $S\downarrow$ refer to spin-up and spin-down channels, respectively.

	3×3		6×3		9×3		12×3		6×6	
	$S\uparrow$	$S\downarrow$	$S\uparrow$	$S\downarrow$	$S\uparrow$	$S\downarrow$	$S\uparrow$	$S\downarrow$	$S\uparrow$	$S\downarrow$
HOL-1(p_z^A)	-1.77	-1.72	-1.11	-1.08	-1.14	-1.15	-0.71	-0.70	-0.78	-0.77
HOL(p_z^B)	-0.79	-0.60	-0.56	-0.50	-0.45	-0.42	-0.40	-0.39	-0.45	-0.43
LUL(p_z^A)	-0.60	-0.62	-0.47	-0.48	-0.40	-0.40	-0.37	-0.37	-0.41	-0.41
LUL+1(p_z^B)	-0.79	-0.60	-0.56	-0.50	-0.45	-0.42	-0.40	-0.39	-0.45	-0.43
HOL-LUL gap	0.19	-0.02	0.09	0.02	0.05	0.02	0.03	0.02	0.04	0.02

3C-SCs) with a single H atom adsorbed were carried out. The calculations were performed by means of the PWSCF code.²⁶ The exchange-correlation energy was computed with the Perdew-Burke-Ernzerhof functional.²⁷ Vanderbilt ultrasoft pseudopotentials replaced the ion cores. The kinetic-energy cutoff was taken at 540 eV. The occupation of the one electron states was calculated at an electronic temperature of $k_B T = 0.01$ eV. The k grid was built using the Monkhorst-Pack scheme²⁸ with maximum spacing between k points of 0.03 \AA^{-1} .

The results of the DFT calculations are shown in Table I. The main difference between the DFT and the TB model results is that the former displays the effect of the spin (i.e., the exchange energy) in the band gap and the appearance of the midgap band. This new midgap band feature cannot be captured by the proposed TB model since the orbital corresponding to the H atom is not introduced explicitly in the TB Hamiltonian [in order to do that the size of the TB matrix should be $2n \cdot m + 1$, instead of $2n \cdot m$] but it is only introduced as a perturbation to the system. HOL-1 of DFT calculations corresponds to a p_z^A linear combination with a strong hybridization with the s orbital of the hydrogen atom. This produces a significant decreasing in its energy (between 0.4 and 1.2 eV below the other three frontier levels in both spin channels, depending on the considered 3C-SC). The HOL, LUL, and LUL+1 of DFT calculations can be identified with the ones obtained through the TB model (the ordering of the levels can vary due to exchange effects). Interestingly, the midgap band crosses the conduction band and thus LUL and LUL+1 are in fact occupied states at the Dirac point, turning the graphene sheet into a metallic system (see Fig. 2). In the spin-up channel a tiny gap, varying from 0.19 eV in the $3\vec{a}_1 \times 3\vec{a}_2$ SC to 0.03 eV in the $12\vec{a}_1 \times 3\vec{a}_2$ SC, is opened between the HOL, and the LUL and LUL+1. This is due to exchange effects not taken into account in the TB model. The effect of exchange is better observed in the density of states of the doped graphene (Fig. 3). It can be noticed that close to the Fermi level the spin-up channel electrons are stabilized with respect to the spin down ones because of the exchange effect. Obviously, the effect of exchange in the gap diminishes when the size of the unit cell increases. In the spin-down channel the valence band and the two conduction bands are almost degenerate at the Dirac point with a gap of 0.02 eV (for all of the studied 3C-SCs) between them. It is worth noticing that the gaps found in the studied 3C-SCs are

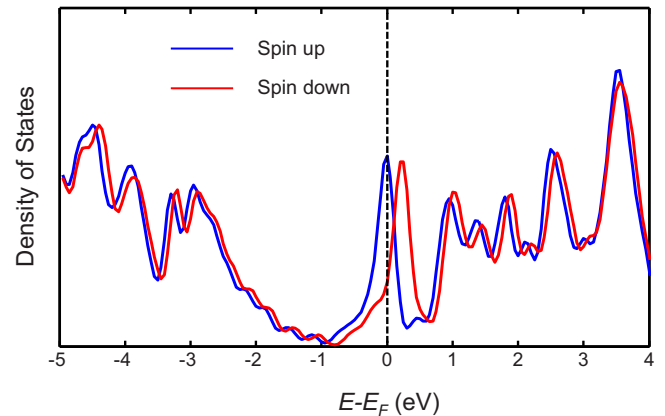


FIG. 3. (Color online) Electronic density of states of a graphene sheet with a hydrogen atom adsorbed with a 3×3 periodicity. The blue curve corresponds to the spin-up channel and the red one to the spin-down channel. The energies are given with respect to the Fermi level.

one or two orders of magnitude smaller than the one found by Duplock *et al.* for the $4\vec{a}_1 \times 4\vec{a}_2$ SC (1.25 eV). This dramatic reduction of the band-gap opening in 3C-SCs leads to the crossing of the midgap and the conduction bands, and eventually to the metallization of the system. Furthermore, this evidences the strong dependence of the band-gap opening of doped graphene with the doping periodicity.

In conclusion, it has been shown that it is possible to minimize the band-gap opening produced by the adsorption of atomic hydrogen on graphene by choosing specific adsorption periodicities. Only a tiny gap is opened in 3C-SCs, due to the small effect of exchange when the H atoms are adsorbed at A_{ij} sites, being $(i-j)$ multiple of 3. This band gap reduction causes in the 3C-SCs the crossing of the conduction and midgap bands, therefore inducing a metallization in the system. These results are also valid for other adsorbates different from atomic hydrogen.

The author thanks Kristian S. Thygesen for useful discussions and Federico Calle-Vallejo for critical reading of the manuscript. This work was supported by the European Union through the FP7 e-I3 ETSF (Contract No. 211956), and THEMA (Contract No. 228539) projects. DFT calculations were carried out in the ARINA cluster.

¹P. R. Wallace, *Phys. Rev.* **71**, 622 (1947).

²K. S. Novoselov, A. K. Geim, S. V. Morozov, D. Jiang, Y. Zhang, S. V. Dubonos, I. V. Grigorieva, and A. A. Firsov, *Science* **306**, 666 (2004).

³A. H. Castro Neto, F. Guinea, N. M. R. Peres, K. S. Novoselov, and A. K. Geim, *Rev. Mod. Phys.* **81**, 109 (2009).

⁴M. Lefevre, E. Proietti, F. Jaouen, and J. P. Dodelet, *Science* **324**, 71 (2009).

⁵A. K. Geim and K. S. Novoselov, *Nature Mater.* **6**, 183 (2007).

⁶N. M. R. Peres, F. Guinea, and A. H. Castro Neto, *Phys. Rev. B*

73, 125411 (2006).

⁷V. M. Pereira, F. Guinea, J. M. B. Lopes dos Santos, N. M. R. Peres, and A. H. Castro Neto, *Phys. Rev. Lett.* **96**, 036801 (2006).

⁸M. Vanin, J. J. Mortensen, A. K. Kelkkanen, J. M. García-Lastra, K. S. Thygesen, and K. W. Jacobsen, *Phys. Rev. B* **81**, 081408 (2010).

⁹Y. H. Lu and Y. P. Feng, *J. Phys. Chem. C* **113**, 20841 (2009).

¹⁰M. Y. Han, B. Ozyilmaz, Y. Zhang, and P. Kim, *Phys. Rev. Lett.* **98**, 206805 (2007).

- ¹¹Y. W. Son, M. L. Cohen, and S. G. Louie, *Phys. Rev. Lett.* **97**, 216803 (2006).
- ¹²R. Balog, B. Jorgensen, L. Nilsson, M. Andersen, E. Rienks, M. Bianchi, M. Fanetti, E. Lægsgaard, A. Baraldi, S. Lizzit, Z. Sljivancanin, F. Besenbacher, B. Hammer, T. G. Pedersen, P. Hofmann, and L. Hornekær, *Nature Mater.* **9**, 315 (2010).
- ¹³D. W. Boukhvalov, M. I. Katsnelson, and A. I. Lichtenstein, *Phys. Rev. B* **77**, 035427 (2008).
- ¹⁴E. J. Duplock, M. Scheffler, and P. J. D. Lindan, *Phys. Rev. Lett.* **92**, 225502 (2004).
- ¹⁵D. C. Elias, R. R. Nair, T. M. G. Mohiuddin, S. V. Morozov, P. Blake, M. P. Halsall, A. C. Ferrari, D. W. Boukhvalov, M. I. Katsnelson, A. K. Geim, and K. S. Novoselov, *Science* **323**, 610 (2009).
- ¹⁶X. Y. Pei, X. P. Yang, and J. M. Dong, *Phys. Rev. B* **73**, 195417 (2006).
- ¹⁷J. Zhou, M. M. Wu, X. Zhou, and Q. Sun, *Appl. Phys. Lett.* **95**, 103108 (2009).
- ¹⁸R. Martinazzo, S. Casolo, and G. F. Tantardini, *Phys. Rev. B* **81**, 245420 (2010).
- ¹⁹S. Casolo, O. M. Lovvik, R. Martinazzo, and G. F. Tantardini, *J. Chem. Phys.* **130**, 054704 (2009).
- ²⁰M. Z. S. Flores, P. A. S. Autreto, S. B. Legoas, and D. S. Galvao, *Nanotechnology* **20**, 465704 (2009).
- ²¹J. O. Sofo, A. S. Chaudhari, and G. D. Barber, *Phys. Rev. B* **75**, 153401 (2007).
- ²²J. C. Charlier, X. Blase, and S. Roche, *Rev. Mod. Phys.* **79**, 677 (2007).
- ²³See supplementary material at <http://link.aps.org/supplemental/10.1103/PhysRevB.82.235418> for auxiliary figures and MATLAB code.
- ²⁴Q. Zhang, H. Yang, C. Zhang, and Z. Ma, *Phys. Rev. B* **73**, 235438 (2006).
- ²⁵J. M. García-Lastra, K. S. Thygesen, M. Strange, and A. Rubio, *Phys. Rev. Lett.* **101**, 236806 (2008).
- ²⁶P. Giannozzi *et al.*, *J. Phys.: Condens. Matter* **21**, 395502 (2009).
- ²⁷J. P. Perdew, K. Burke, and M. Ernzerhof, *Phys. Rev. Lett.* **77**, 3865 (1996).
- ²⁸H. J. Monkhorst and J. D. Pack, *Phys. Rev. B* **13**, 5188 (1976).